ChemComm

COMMUNICATION

View Article Online
View Journal | View Issue

Cite this: *Chem. Commun.*, 2020, **56**, 12550

Received 7th June 2020,
Accepted 2nd September 2020

DOI: 10.1039/d0cc03983g

rsc.li/chemcomm

Dual emitting Ag_{35} nanocluster protected by 2-pyrene imine thiol†

Arijit Jana, [ab] Papri Chakraborty, [a] Wakeel Ahmed Dar,[a] Sourov Chandra, [b] Esma Khatun, [a] M. P. Kannan, [a] Robin H. A. Ras [bc] and Thalappil Pradeep *[a]

In this communication, we present the synthesis of 2-pyrene imine thiol (2-PIT)-protected Ag_{35} nanoclusters using a ligand exchange-induced structural transformation reaction. The formation of the nanocluster and its composition were confirmed through several spectroscopic and electron microscopic studies. The UV-vis absorption spectrum showed a set of characteristic features of the nanocluster. This nanocluster showed blue emission under UV light due to pyrene to metal core charge-transfer, and NIR emission due to charge-transfer within the metal core. This is the first report on dual emitting pyrene protected atomically precise silver nanoclusters.

Ligand protected metal nanoclusters (NCs) are an emerging class of quantum materials connecting the gap between atoms and bulk metallic materials.[1,2] Owing to their unique electrical, optical and other spectroscopic properties such as luminescence,[3–5] chirality,[6] *etc.*, they are important for applications such as catalysis,[7] CO_2 reduction,[8] bioimaging,[9] *etc.* The surface ligand environment not only stabilizes their fragile metal core but also determines their electronic properties.[10,11] The literature suggests that small organic thiol and phosphene co-protected silver nanoclusters such as Ag_6,[12] Ag_{14},[13] Ag_{25},[14] Ag_{29},[15] Ag_{67},[16] *etc.*, are more promising compared to bulky DNA[17,18] and dendrimer[19] protected NCs in making structure–property correlations. Our group has reported silver NCs such as Ag_{16}, Ag_{17},[20] Ag_{22},[21] Ag_{40}, Ag_{46},[22] *etc.*, and their crystal structures as a step toward understanding their various functional properties. Generally, the light sensitivity and chemical instability of the Ag core limit their practical applications. In view of such limitations, designing new multidentate ligands that can stablize Ag NCs is important. In contrast to conventional organic thiols and phosphines used for protecting silver NCs, in this work we have used 2-pyrene imine thiol, a polycyclic aromatic hydrocarbon (PAH)-based ligand for Ag NC synthesis. Atomically precise silver NCs protected with electron dense pyrene ligands are a new class of functional hybrid nanomaterials, which show electronic, optical and other physical properties, due to a combination of both the ligand and the cluster core.

Pyrene is a good candidate among other PAHs, due to its multiple absorption and emission properties.[23] Due to their high emission quantum yield and excimer stability, pyrene functionalised nanoparticles (NPs) and dendrimers are widely used in optoelectronic,[24,25] molecular labelling,[26] and fluorescence sensing applications.[27] There are some reports on functionalised pyrene protected gold NPs, wherein the NPs show erratic emission of pyrene.[28] Due to the resonance energy transfer from the chromophore to the metallic core, the emission quenches significantly. The distance from the nanoparticle core to pyrene has a significant role in this energy transfer process.[29] Generally, increasing the distance from the metallic core to the pyrene center decreases quenching. In the case of a cluster, which has a molecular core, quenching is expected.

To obtain a highly stable silver NC, appended with PAHs, we have used 2-PIT and triphenylphosphine (TPP) as ligands. The synthesis of the 2-PIT ligand was through a high-temperature condensation reaction between pyrene aldehyde and 2 amino thio-phenol. Fig. 1a shows a schematic representation of the synthesis of the 2-PIT ligand. In brief, pyrene aldehyde was mixed with 2 amino thio-phenol in an argon atmosphere in a methanol-ethanol solvent mixture, under refluxed (60 °C) conditions. After 4 hour of reaction, a yellow colored ligand was filtered using a Whatman 42 filter paper and washed several times with the methanol–ethanol solvent mixture to remove excess starting materials. The as-prepared 2-PIT ligand was confirmed using ^1H and $^{13}C\{^1H\}$ NMR (shown in Fig. S1 and S2 respectively, ESI†) and mass spectral studies.

The formation of the 2-PIT ligand was confirmed through single-crystal structure studies. Fig. 1b shows the crystal structure

[a] *Department of Chemistry, DST Unit of Nanoscience (DST UNS) and Thematic Unit of Excellence (TUE), Indian Institute of Technology Madras, Chennai 600036, India. E-mail: pradeep@iitm.ac.in*
[b] *Department of Applied Physics, Aalto University, School of Science, Puumiehenkuja 2, 02150, Espoo, Finland*
[c] *Department of Bioproducts and Biosystems, Aalto University School of Chemical Engineering, 02150, Espoo, Finland*

† Electronic supplementary information (ESI) available: Experimental details of synthesis and characterization. CCDC 2008467. For ESI and crystallographic data in CIF or other electronic format see DOI: 10.1039/d0cc03983g

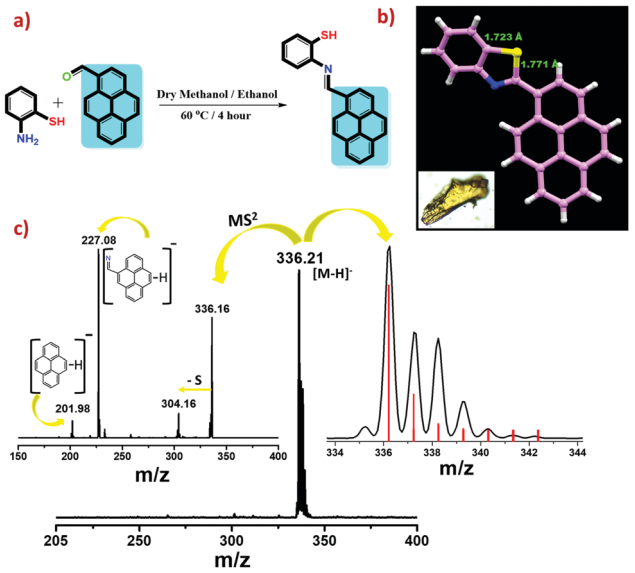

Fig. 1 (a) Schematic representation of the synthesis of the 2-pyrene imine thiol ligand; (b) the crystal structure of the ligand (inset shows the optical image of the single crystal); (c) the mass spectrum and the MS/MS fragmentation data of the ligand (color codes of the atoms: violet = carbon; blue = nitrogen; yellow = sulphur; and gray = hydrogen).

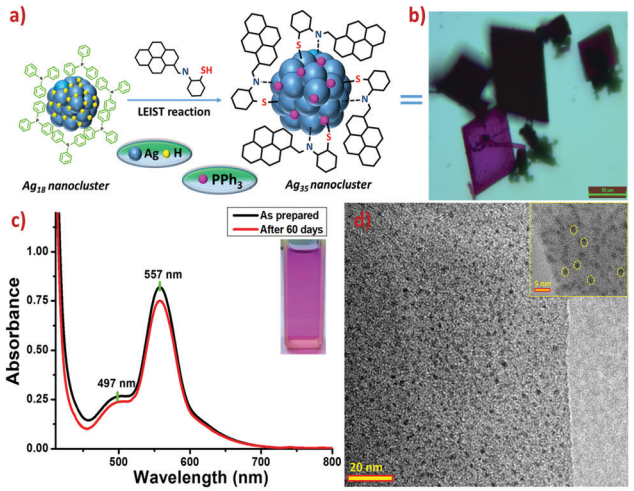

Fig. 2 (a) Schematic representation of the synthesis of Ag_{35} NC by a LEIST reaction; (b) the optical microscopic image of the Ag_{35} NC crystals; (c) the UV-Visible absorption spectrum of Ag_{35} NC showing its stability (inset shows the photographic image of the NC solution in DCM); (d) the TEM image of the NC showing uniform particle distribution (inset shows the HRTEM image of the NCs, and some particles are encircled).

of the ligand, which crystallized in the monoclinic $P2_1/c$ crystal system. From the crystal structure, we observed that the C–H proton of the imine group and the S–H proton combined themselves and formed a five-membered ring. The distance of S and imine carbon is 1.77 Å compared to 1.72 Å distance of the C–S bond with the benzene ring, which indicates weak bonding with the imine carbon. Several C–H–Π intermolecular interactions in the intermolecular packing of the ligands are shown in Fig. S3 (ESI†); four molecules packed inside the unit cell in a lamellar fashion are visible. The negative mode electrospray ionisation mass spectrum (ESI-MS) in DCM showed a $[M - H]^-$ ion peak at m/z 336.21, which indicated the existence of the molecule in the thiol (SH) form in solution. The proton NMR spectrum shown in Fig. S1 (ESI†) with a single peak at 3.45 ppm confirmed the thiol form in solution. Furthermore, we confirmed the formation of the imine thiol form through MS/MS fragmentation studies, showing the loss of S, pyrene imine and pyrene moieties from the molecular ion peak, by varying the collision energy.

The Ag_{35} NC was prepared using a ligand exchange-induced structural transformation (LEIST) reaction from the Ag_{18} nanocluster. Fig. 2a shows a schematic representation of the synthetic procedure employed in the LEIST reaction. Product clusters were also formed by a controlled co-reduction reaction of metal thiolates in the presence of TPP. Detailed characterization of the Ag_{18} NCs through UV-vis absorption and MS studies is shown in Fig. S4 (ESI†). The conversion of Ag_{18} NC to Ag_{35} NC through several intermediates was reflected in the changing color of the reaction mixture. The changes in the UV-vis absorption features of these intermediates are shown in Fig. S5 (ESI†). A dark violet color appeared at the end of the reaction after 48 h. Fig. 2b shows the UV-vis absorption features of the purified NC. The nanocluster has well-defined sharp absorption features at 557 and 497 nm. The absorption features of the Ag_{35} NC remain unchanged after two months, indicating the good stability of the NC. The uniform particle size distribution of the NC was also confirmed using TEM imaging. The TEM images show small cluster particles <2 nm in diameter (Fig. 2d).

The molecular composition of this NC was confirmed using the high resolution ESI-MS (HR ESI-MS) technique. During ESI-MS measurements, the ionization of the cluster was enhanced by adding a few drops of methanol. The instrumentation details are given in the ESI.† The full range mass spectrum shown in Fig. 3a indicates a sharp peak at m/z 2659.7 in the 3+ charge state. This corresponds to a mass of 7971.1 for the molecular ion species. This peak was assigned as $[Ag_{35}(2\text{-PIT})_7(TPP)_7@(H_2O)]^{3+}$ by comparing its experimental isotopic distribution with the isotopic distribution of the simulated spectrum. The assignment was further verified using collision induced dissociation (CID) mass spectrometry measurements at different collision-energies (CEs), which are instrumental units of the Waters Synapt G2 Si mass spectrometer. The MS/MS fragmentation patterns are shown in Fig. 3b. From the MS/MS spectra, we observed that by varying the CE from 0 to 50, there were four sequential mass losses of 262 units, which indicates four TPP unit detachments from the cluster. Next, by increasing the CE from 50 to 150, further loss of TPP was not observed, which suggested that only 4 TPP molecules are weakly bonded to the outer shell of the cluster. At CE 150, a new peak appeared at 2755.5 with the 2+ charge state. The mass loss of 2468.18 indicated the loss of the $[Ag_{13}(H_2O)(TPP)_4]$ fragment from the molecular ion peak. Next upon increasing the CE from 150 to 175, we observed further loss of three TPPs, which indicated that while four TPP molecules are loosely bound to the cluster surface, there were three other strongly bound TPP molecules. Upon further increasing the CE, five sequential mass losses of 124 units due to the loss of the aminothiophenol moities

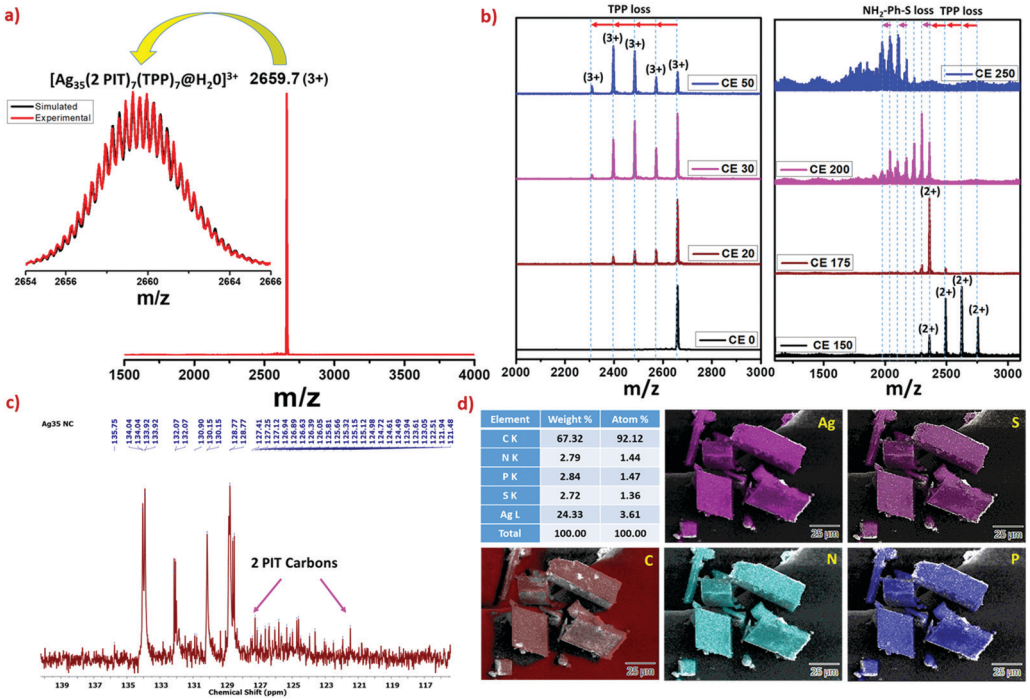

Fig. 3 (a) Positive mode ESI-MS spectrum of the Ag_{35} NC in DCM (inset shows the simulated and experimental isotopic distribution patterns of the 2659.7 peak); (b) MS/MS fragmentation pattern of the 2659.7 peak using different collision energies; (c) $^{13}C\{^{1}H\}$ NMR spectrum of the Ag_{35} NC in $CDCl_3$; (d) SEM EDS elemental mapping of NC crystals indicating their atomic composition.

from the NC, generated by the fragmentation of the 2-PIT ligand, were seen.

To further understand the binding of TPP and 2-PIT ligands, we studied the ^{13}C and ^{31}P NMR spectra of the NC. Fig. 3c shows the ^{13}C NMR spectrum of the NCs, which exhibited 23 low intensity signature peaks of carbon in the 120–128 ppm window due to 2-PIT along with TPP signature peaks in the 128–135 ppm region. This clearly suggested the co-protection of the 2-PIT and TPP ligands. Multiplet peak splitting of the ^{13}C spectrum for the TPP region is most probably due to the variation in the chemical environment of the TPP outside the NC surface. The broad ^{31}P NMR signal at 9.32 ppm shown in Fig. S6 (ESI†) indicated TPP binding with the cluster. Although there are two sets of TPP molecules on the cluster surface, we were not able to distinguish between them through the ^{31}P NMR spectrum. The XPS spectra are shown in Fig. S7 and S8 (Table S3) (ESI†) of the ligand and Ag_{35} NC, respectively. Among the four peaks of Ag_{35} NC, two peaks at 284.8 and 286.6 eV are comparable with the two peaks at 284.8 and 286.3 eV of the C 1s region of the 2-PIT ligand, which suggests the binding of the 2-PIT ligand. The two other peaks of the C 1s region at 288.2 and 289.4 eV are due to the two types of TPP ligands. The decrease in the binding energy of the N 1s and S 2p regions in the Ag_{35} NC, compared to the 2-PIT ligand, is probably due to the electron back donation from the metal core to the N and S end of the ligand. The higher electronegativity of N and S compared to Ag is also the reason behind it. The binding energy of 368.4 and 374.5 eV for the Ag 3d region suggests the metallic state of silver.

Although the as-grown cubical blackish-violet crystals of the NC showed optical polarisation, due to the lack of intense electron diffraction spots, we were not able to get the single-crystal structure of the NCs. Fig. 2b and Fig. S9 (ESI†) show the optical microscopic images of the single crystals grown after crystallization. The EDS elemental images of the single crystals are shown in Fig. 3d. The single crystal showed the existence of Ag, S, P, N and C in an atomic ratio of 3.61 : 1.36 : 1.47 : 1.44 : 92.12 in the crystal, which indicated the co-existence of 2-PIT and TPP ligands in the NC. The FTIR spectra of the 2-PIT ligand and Ag_{35} NC are shown in Fig. S10 (ESI†). The sharp feature at 3049 cm^{-1} corresponded to the pyrene C–H stretching mode. Similar vibrational features are also observed there for the 2-PIT ligand. The broad O–H vibrational feature centered at 3435 cm^{-1} indicated that H_2O is present in the NC.

Interestingly, the Ag_{35} nanocluster exhibits dual emission features in blue (449 nm) and NIR (896 nm) regions upon excitation at 417 and 530 nm, respectively (Fig. 4). Fig. 4a shows the excitation spectrum of the Ag_{35} NCs at 449 nm emission, demonstrating three major excitation peaks at 297, 365 and 417 nm. These low lying excitation maxima resembling the absorption maxima of the 2-PIT ligand are due to the charge transfer from pyrene to the metal core. The NIR emission peak at 896 nm corresponding to the excitation maxima at 530 and 558 nm is due to the metal shell to metal core charge tranfer (MMCT) in the NC. Comparing the absorption maximum at 557 nm with the excitation maxima, we can conclude that the NIR emission is due to the charge transfer within the metal core.[30] A similar type of MMCT leading to NIR emission was

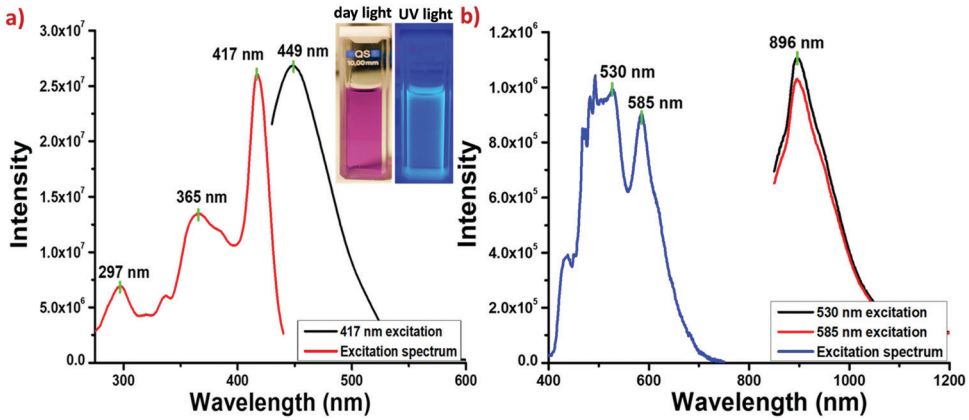

Fig. 4 (a) Photoluminescence excitation and emission spectra of the nanocluster (inset shows images of the cluster solution under day light and UV light) and (b) NIR emission and the corresponding excitation spectra of the nanocluster.

reported in the literature.[31] The Ag_{35} nanocluster shows a dual emissive character of the ligand as well as the metal core and is the first example showing this behavior.

In conclusion, we have shown the synthesis of a 2-pyrene imine thiol protected Ag_{35} nanocluster using a LEIST reaction. The formation of the NC was confirmed using UV-vis absorption spectroscopy, mass spectrometry, and multinuclear NMR, TEM, SEM, EDS, FTIR and XPS measurements. The cluster showed intense blue emission due to pyrene to metal core electron-transfer in the solution phase. There was also a comparable NIR emission observed due to metal-to-metal charge transfer. This work is a step toward making silver nanoclusters with a family of electron rich pyrene molecules having composite electronic features. Dual emission in such types of materials may be tuned for desired applications such as ion sensing and bio imaging.

This work was supported by the SPARC scheme, Govt. Of India through the grant, SPARC/2018-2019/P910/SL. The authors would like to thank the Sophisticated Analytical Instrument Facility, IIT Madras (SAIF, IITM), for single crystal XRD measurement. AJ acknowledges financial support from IIT Madras.

Conflicts of interest

There are no conflicts to declare.

Notes and references

1 R. Jin, C. Zeng, M. Zhou and Y. Chen, *Chem. Rev.*, 2016, **116**, 10346–10413.
2 I. Chakraborty and T. Pradeep, *Chem. Rev.*, 2017, **117**, 8208–8271.
3 X. Kang and M. Zhu, *Chem. Soc. Rev.*, 2019, 2422–2457.
4 Z. Wang, J. W. Liu, H. F. Su, Q. Q. Zhao, M. Kurmoo, X. P. Wang, C. H. Tung, D. Sun and L. S. Zheng, *J. Am. Chem. Soc.*, 2019, **141**, 17884–17890.
5 Z. Wang, H. Su, Y. Tan, S. Schein, S. Lin, W. Liu, S. Wang, W. Wang, C. Tung, D. Sun and L. Zheng, *Proc. Natl. Acad. Sci. U. S. A.*, 2017, **114**, 12132–12137.
6 Y. Chen, C. Liu, Q. Tang, C. Zeng, T. Higaki, A. Das, D. Jiang, R. N. Rosi and J. Rongchao, *J. Am. Chem. Soc.*, 2016, **138**, 1482–1485.
7 Y. Wu, D. Wang and Y. Li, *Chem. Soc. Rev.*, 2014, **43**, 2112–2124.
8 Y. Liu, X. Chai, X. Cai, M. Chen, R. Jin, W. Ding and Y. Zhu, *Angew. Chem., Int. Ed.*, 2018, **130**, 1–6.
9 Z. Luo, K. Zheng and J. Xie, *Chem. Commun.*, 2014, **50**, 5143–5155.
10 J. Liu, Z. Wang, Y. Chai, M. Kurmoo, Q. Zhao, X. Wang, C. Tung and D. Sun, *Angew. Chem., Int. Ed.*, 2019, **58**, 6276–6279.
11 Z. Wang, H. Su, C. Tung and D. Sun, *Nat. Commun.*, 2018, **9**, 4407.
12 Z. Han, X. Dong, P. Luo, S. Li, Z. Wang, S. Zang and T. C. W. Mak, *Sci. Adv.*, 2020, **6**, 1–9.
13 Z. Wang, M. Wang, Y. Li, P. Luo, T. Jia, R. Huang, S. Zang and T. C. W. Mak, *J. Am. Chem. Soc.*, 2018, **140**, 1069–1076.
14 C. P. Joshi, M. S. Bootharaju, M. J. Alhilaly and O. M. Bakr, *J. Am. Chem. Soc.*, 2015, **137**, 11578–11581.
15 L. G. Abdulhalim, M. S. Bootharaju, Q. Tang, S. Del Gobbo, R. G. Abdulhalim, M. Eddaoudi, D. Jiang and O. M. Bakr, *J. Am. Chem. Soc.*, 2015, **137**, 11970–11975.
16 M. J. Alhilaly, M. S. Bootharaju, C. P. Joshi, T. M. Besong, A. Emwas, R. Juarez-mosqueda, S. Kaappa, S. Malola and K. Adil, *J. Am. Chem. Soc.*, 2016, **138**, 14727–14732.
17 S. Y. New, S. T. Lee and X. D. Su, *Nanoscale*, 2016, **8**, 17729–17746.
18 Z. Yuan, Y. Chen, H. Li, H. Chang and Y. Chen, *Chem. Commun.*, 2014, **50**, 9800–9815.
19 W. Lesniak, A. U. Bielinska, K. Sun, K. W. Janczak, X. Shi, J. R. Baker Jr and L. P. Balogh, *Nano Lett.*, 2005, **5**, 2123–2130.
20 W. A. Dar, M. Bodiuzzaman, D. Ghosh, G. Paramasivam, E. Khatun, K. S. Sugi and T. Pradeep, *ACS Nano*, 2019, **13**, 13365–13373.
21 E. Khatun, M. Bodiuzzaman, K. S. Sugi, P. Chakraborty and T. Pradeep, *ACS Nano*, 2019, **13**, 5753–5759.
22 M. Bodiuzzaman, A. Ghosh, K. S. Sugi, A. Nag, E. Khatun, B. Varghese, G. Paramasivam and T. Pradeep, *Angew. Chem., Int. Ed.*, 2018, **57**, 1–7.
23 F. M. Winnik, *Chem. Rev.*, 1993, **93**, 587–614.
24 T. M. Figueira-duarte and M. Klaus, *Chem. Rev.*, 2011, **111**, 7260–7314.
25 F. Zinna, S. Voci, L. Arrico, E. Brun, A. Homberg, L. Bouffier, T. Funaioli, J. Lacour, N. Sojic and L. Di Bari, *Angew. Chem., Int. Ed.*, 2019, **58**, 6952–6956.
26 U. Drechsler, B. Erdogan and V. M. Rotello, *Chem. – Eur. J.*, 2004, **10**, 5570–5579.
27 A. Senthamizhan, A. Celebioglu, S. Bayir, M. Gorur, E. Doganci, F. Yilmaz and T. Uyar, *ACS Appl. Mater. Interfaces*, 2015, **7**, 21038–21046.
28 G. Battistini, P. G. Cozzi, J. Jalkanen, M. Montalti, L. Prodi, N. Zaccheroni and F. Zerbetto, *ACS Nano*, 2008, **2**, 77–84.
29 K. G. Thomas and P. V. Kamat, *Acc. Chem. Res.*, 2003, **36**, 888–898.
30 Z. Guan, J. Zeng, Z. Nan, X. Wan, Y. Lin and Q. Wang, *Sci. Adv.*, 2016, **1**, 1–8.
31 F. Tian and R. Chen, *J. Am. Chem. Soc.*, 2019, **141**, 7107–7114.